Buckling Analysis of Porous Functionally Graded Plates

Anil Kumar Gupta
Department of Civil Engineering, National Institute of Technology Patna, India
anilguptakeck@gmail.com (corresponding author)

Ajay Kumar
Department of Civil Engineering, National Institute of Technology Delhi, India
sajaydce@gmail.com

Received: 11 April 2023 | Revised: 23 April 2023 | Accepted: 27 April 2023

 DOI: https://doi.org/10.48084/etasr.5943

ABSTRACT

This study investigated the buckling behavior of Porous Functionally Graded Material (PFGM) plates. The present model assumes unevenly distributed porosity along the plate thickness and the use of the novel hyperbolic shear deformation functions and hyperbolic tangent and secant thickness stretching functions. In the present work, a porous Functionally Graded (FG) plate was analyzed by the principle of virtual work in order to understand the buckling behavior under uniaxial and biaxial compressive loading. The Rayleigh quotient method was applied to find the critical buckling load. The mesh convergence was investigated on a Finite Element (FE) model, and the accuracy of the results was compared with the prior research. The results of the proposed model match reasonably well with the ones of the published literature. Thorough parametric studies were performed to investigate the effect of porosity on the critical buckling load of the PFGM plate.

Keywords-FG porous plate; finite element method; buckling load; porosity

I. INTRODUCTION

The expansion of modern society's infrastructure has created the need for new smart building materials, which ought to be more readily available, safer, and more ecologically friendly. Numerous investigations on Functionally Graded Material (FGM) beams, plates, and shells have been carried out [1, 2]. Structures with graded porosity have inserted pores into the microstructure to satisfy the required structural performance by customizing the local density of the structure, are one of the most recent innovations in FGM. FGM has a progressive change in composition along the volume, which causes gradual changes in the mechanical material's characteristics. In a variety of technical applications, PFGMs have significant potential. For instance, graded metal foam presents special promise for lightweight construction in the civil, automotive, and aerospace industries [3, 4]. Additionally, PFGMs are the ideal choice for structures under dynamic or impact loads due to their great energy-absorbing capacity [5, 6]. Despite its practical significance, research in this developing field is still in its infancy and fairly sparse, with the majority of earlier work focused on the compression behavior [7, 8]. For the porous materials model, a progressive change in material characteristics results from the change in porosity over the thickness direction of the structures. So, scientists and researchers have paid much attention to structures composed of porous-cellular materials [9].

In order to investigate more the annular sectorial porous plates' respond to evenly distributed in-plane compressive pressure in terms of buckling and vibration, authors in [10] suggested an analytical method. Many shear deformation theories have been proposed, using various shape functions, and assumptions to developed high-order shear theory (HSDT) using a sinusoidal function for FG sandwich members [11-13]. Using classical plate theory, authors in [14] examined the buckling modes of rectangular FG plates subjected to in-plane stress. Mechanical and thermal loads were applied on FG circular plates, and nonlinear bending and post-buckling behavior were analyzed by Von Karman nonlinearity. The result shows that FG plates have good resistance against thermal load or a combination of mechanical and thermal loads than the fully metallic plates [15]. The post-buckling behavior of imperfect nanobeams formed of metal foam with different porosity distributions was studied in [16]. Authors in [17, 18] used the traditional plate theory to examine thermal and mechanical buckling of FG circular plates constructed of porous material. Buckling analysis of FG plates with two different kinds of thermal loads was discussed in [19]. Authors in [20] investigated the impact of evenly and unevenly distributed porosity on the critical buckling load in the FG plates and constructed a mathematical model.

The current work investigates the uniaxial and biaxial compression behavior of PFGM plates using hyperbolic shear deformation functions and hyperbolic tangent and secant thickness stretching functions. There is a need to develop a simple two-dimensional model to analyze the buckling behavior of porous FGM plates. Hence, in the current work, a C_0 FE model is created based on the new mathematical model for simplifying buckling analysis. The FE model was tested for convergence and the obtained results were validated with the literature. The buckling behavior was investigated parametrically to examine the effect of porosity with variations of the side to thickness ratio.

II. FORMULATION

A. Geometry of the Porous FG Plate

Figure 1 shows the geometrical characteristics of the porous FG plate whose length, width, and thickness are a, b, and h, respectively, and which has unevenly distributed porosity. The mid-plane of the plate is taken as the reference plane (z = 0).

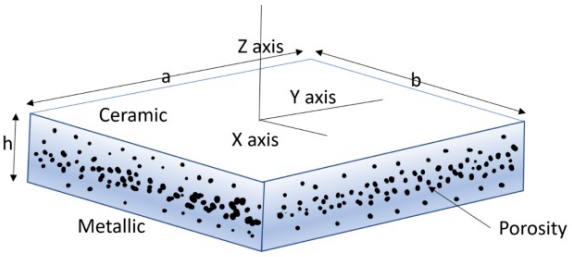

Fig. 1. Geometry of the porous FG plate.

B. Homogenization of the FG Plate

Effective material parameter like Young's modulus $E(z)$ and Poisson ratio $\mu(z)$, can be determined as a function of thickness coordinates from the mid-plane. Voigt's rule of mixture homogenization technique is utilized to determine the mechanical characteristics of the PFGM plate, considering unevenly porosities across the plate thickness direction, effective properties can be determined as follows:

$$E(z) = E_{met} + (E_{Cr} - E_{met}) * \left\{\frac{1}{2} + \frac{z}{h}\right\}^{p} - \xi\frac{(E_{Cr}+E_{met})}{2}\left(1 - 2\frac{|z|}{h}\right) \quad (1)$$

$$\mu(z) = \mu_{met} + (\mu_{Cr} - \mu_{met}) * \left\{\frac{1}{2} + \frac{z}{h}\right\}^{p} - \xi\frac{(\mu_{Cr}+\mu_{met})}{2}\left(1 - 2\frac{|z|}{h}\right) \quad (2)$$

where E_{met}, μ_{met} and E_{cr}, μ_{cr} are the Young's modulus and Poission's ratio of metal and ceramic, respectively. Power index ($p \geq 0$) equal to zero corresponds to the purely ceramic state. V_{cr} is the ceramic volume fraction and V_{met} is the metallic volume fraction. Their relation is: $V_{cr} + V_{met} = 1$

The proposed HSDT uses the shear deformation function f(z) associated with β_{sx} and β_{sy} which is represented in (3). To define the transverse shear strain distribution along the plate thickness, the thickness stretching function t(z) associated with ϕ is expressed in (4) to include the thickness stretching deformation of the plate.

$$f(z) = z\cosh\left\{\frac{1}{2}\right\} - h\sinh\left\{\frac{z}{h}\right\} \quad (3)$$

$$t(z) = \left\{\frac{3\pi}{2}\right\}\left(1 - \tanh^2\frac{z}{h}\right) - \frac{3\pi}{2}\operatorname{sech}^2\frac{1}{2} \quad (4)$$

In-plane displacements u, v, and transverse displacement w are expressed in (5)-(7) using the shape function f(z) and thickness stretching function t(z). For C_0 continuity of the FE analysis, the out of plane derivatives are complex due to the involvement of the strain with the second-order derivatives, but C_1 continuity is extremely intricate and difficult to model. Therefore, new nodal unknowns are substituted for the out-of-plane derivatives to verify that the displacement field variables are continuous within the elements and need the application of the penalty approach during the FE formulation.

$$u(x,y,z) = u_0(x,y) - z\alpha_{bx}(x,y) - \left\{z\cosh\left\{\frac{1}{2}\right\} - h\sinh\left\{\frac{z}{h}\right\}\right\}\beta_{sx}(x,y) \quad (5)$$

$$v(x,y,z) = v_0(x,y) - z\alpha_{by}(x,y) - \left\{z\cosh\left\{\frac{1}{2}\right\} - h\sinh\left\{\frac{z}{h}\right\}\right\}\beta_{sy}(x,y) \quad (6)$$

$$w(x,y,z) = w_0(x,y) + \left\{\left\{\frac{3\pi}{2}\right\}\left(1 - \tanh^2\frac{z}{h}\right) - \frac{3\pi}{2}\operatorname{sech}^2\frac{1}{2}\right\}\phi(x,y) \quad (7)$$

where $\alpha_{bx} = \frac{\partial w}{\partial x}$, $\alpha_{by} = \frac{\partial w}{\partial y}$.

C. Kinematics of Structure

The strain–displacement connection is derived by differentiating the displacement field equations as given below:

$$\begin{aligned}
\epsilon_{xx} &= \frac{\partial u_o}{\partial x} - z\frac{\partial \alpha_{bx}}{\partial x} - f(z)\frac{\partial \beta_{sx}}{\partial x}\\
\epsilon_{yy} &= \frac{\partial v_o}{\partial y} - z\frac{\partial \alpha_{by}}{\partial y} - f(z)\frac{\partial \beta_{sy}}{\partial y}\\
\epsilon_{zz} &= \frac{\partial t_z}{\partial z}\phi\\
\gamma_{xy} &= \left\{\frac{\partial u_o}{\partial y} + \frac{\partial v_o}{\partial x}\right\} - z\left\{\frac{\partial \alpha_{bx}}{\partial y} + \frac{\partial \alpha_{by}}{\partial x}\right\} - f(z)\left\{\frac{\partial \beta_{sx}}{\partial y} + \frac{\partial \beta_{sy}}{\partial x}\right\}\\
\gamma_{xz} &= \frac{\partial w_0}{\partial x} - \alpha_{bx} - \frac{\partial f_z}{\partial z}\beta_{sx} + t(z)\frac{\partial \phi}{\partial x}\\
\gamma_{yz} &= \frac{\partial w_0}{\partial y} - \alpha_{by} - \frac{\partial f_z}{\partial z}\beta_{sy} + t(z)\frac{\partial \phi}{\partial y}
\end{aligned} \quad (8)$$

D. Constitutive Relations for the Porous FG Plate

The linear constitutive relationship between stresses and strain is given by the constitutive matrix.

$$Q_{11} = Q_{22} = Q_{33} = \frac{E(z)(1-\mu^2)}{1-3\mu^2-2\mu^3}$$

$$Q_{12} = Q_{13} = Q_{23} = \frac{E(z)\mu(1+\mu)}{1-3\mu^2-2\mu^3} \quad (9)$$

$$Q_{44} = Q_{55} = Q_{66} = \frac{E(z)}{2(1+\mu)}$$

$$\begin{Bmatrix} \sigma_{xx} \\ \sigma_{yy} \\ \sigma_{zz} \\ \tau_{xy} \\ \tau_{xz} \\ \tau_{yz} \end{Bmatrix} = \begin{bmatrix} Q_{11} & Q_{12} & Q_{13} & 0 & 0 & 0 \\ Q_{12} & Q_{22} & Q_{23} & 0 & 0 & 0 \\ Q_{13} & Q_{23} & Q_{33} & 0 & 0 & 0 \\ 0 & 0 & 0 & Q_{44} & 0 & 0 \\ 0 & 0 & 0 & 0 & Q_{55} & 0 \\ 0 & 0 & 0 & 0 & 0 & Q_{66} \end{bmatrix} \begin{Bmatrix} \epsilon_{xx} \\ \epsilon_{yy} \\ \epsilon_{zz} \\ \gamma_{xy} \\ \gamma_{xz} \\ \gamma_{yz} \end{Bmatrix} \quad (10)$$

E. Equations of Motion

Euler-Lagrange equations of motion can be derived by applying the virtual work principle to the strain energy (U), the external work done by compressive forces (C), and the artificial constraint (R) of PFGM plate system as shown in (11):

$$\oint \delta(U + R - C)\, \partial\Omega = 0 \quad (11)$$

The strain energy of the PFGM plate is shown in (12):

$$U = \frac{1}{2}\iiint \epsilon^T \sigma\, \partial x\, \partial y\, \partial z$$

$$= \frac{1}{2}\iint \epsilon_0{}^T \{\int Z^T [Q_{ij}] Z\, \partial z\} \epsilon_0\, \partial x\, \partial y \quad (12)$$

The critical buckling load along x and y axes is represented by Nx and Ny, while Nxy represents shear buckling. The total work done by the external compressive forces acting on the plate edges:

$$V = \frac{1}{2}\iiint \left\{ N_x \frac{\partial w^2}{\partial x} + N_y \frac{\partial w^2}{\partial y} + 2N_{xy} \frac{\partial w}{\partial x}\frac{\partial w}{\partial y} \right\} dxdydz \quad (13)$$

The material rigidity matrix [D] is obtained from the constitutive matrix given in (10) and the thickness matrix given in (14). This matrix facilitates the use of the proposed HSDT as an equivalent single layer theory to downscale the 3-D domain to the 2-D domain for the analysis.

$$[Z] = \begin{bmatrix} 1 & 0 & 0 & 0 & 0 & z & 0 & 0 & 0 & 0 & f_z & 0 & 0 & 0 & 0 & 0 & 0 & 0 \\ 0 & 1 & 0 & 0 & 0 & 0 & z & 0 & 0 & 0 & 0 & f_z & 0 & 0 & 0 & 0 & 0 & 0 \\ 0 & 0 & 0 & 0 & 0 & 0 & 0 & 0 & 0 & 0 & 0 & 0 & 0 & 0 & 0 & t'_z & 0 & 0 \\ 0 & 0 & 1 & 0 & 0 & 0 & 0 & z & 0 & 0 & 0 & 0 & f_z & 0 & 0 & 0 & 0 & 0 \\ 0 & 0 & 0 & 1 & 0 & 0 & 0 & 0 & 1 & 0 & 0 & 0 & 0 & f'_z & 0 & 0 & t_z & 0 \\ 0 & 0 & 0 & 0 & 1 & 0 & 0 & 0 & 0 & 1 & 0 & 0 & 0 & 0 & f'_z & 0 & 0 & t_z \end{bmatrix} \quad (14)$$

$$[D] = \int_{z=-h/2}^{z=h/2} [Z]^T \left[Q_{ij}\right] [Z]\, \partial z \quad (15)$$

The geometric rigidity matrix $[D_G]$ is obtained by $[\widehat{N}]$ and the thickness coordinate matrix $[Z_b]$:

$$[D_G] = \int_{z=-h/2}^{z=h/2} [Z_b]^T \left[\widehat{N}\right] [Z_b]\, \partial z \quad (16)$$

where: $[\widehat{N}] = \begin{bmatrix} N_x & N_{xy} \\ N_{xy} & N_y \end{bmatrix}$, $[Z_b] = \begin{bmatrix} 1 & 0 \\ 0 & 1 \\ t(z) & 0 \\ 0 & t(z) \end{bmatrix}$

The displacement in the FE model can be represented as the linear combination of node shapes and corresponding shape functions. The material stiffness matrix and the geometrical stiffness matrix are expressed in (17) and (18), respectively. [J] is the Jacobian matrix of the system, $[J] = \partial(x,y)/\partial(\zeta,\eta)$.

$$[K] = \iint [B]^T [D] [B]\, [J]\ \partial\zeta\, \partial\eta \quad (17)$$

$$[K_G] = \iint [B_B]^T [D_G] [B_B]\, [J]\ \partial\zeta\, \partial\eta \quad (18)$$

III. RESULTS AND DISCUSSION

In this work, buckling analysis of porous FG plate was carried out using the FE formulation based on the nine-node isoparametric C_0 continuous shape function.

A. Model Convergence and Validation

Based on the suggested innovative HSDT, the governing equations for the FE model, which is utilized for the buckling analysis of the PFGM plate, are obtained from the principle of virtual work. In-house MATLAB algorithm for FE formulation is written using the nine-noded Lagrangian isoparametric shape functions. Using mesh convergence studies, the FE model is evaluated and its performance is assessed. The FE analysis is carried out on simply supported square (SSSS) PFGM plate. The material properties are shown in Table I. To predict the buckling response of the PFGM plate, we consider the plate to be subjected to axial in-plane forces.

TABLE I. MATERIAL PROPERTIES

Material	Poission's ratio	Density (kg/m^3)	Modulus of elastiity (GPa)
Al_2O_3	0.3	2702	70
Al	0.3	3800	380

To investigate the change in the dimensionless critical buckling load with various power law indices, different uneven porosity distribution types and mesh sizes were considered. The numerical solutions are computed using the novel theory, and the results are compared with the ones in the literature. The non-dimensional critical buckling ratio is expressed as:

$$N_{cr} = \frac{N \times a^2}{E_m h^3} \quad (19)$$

where N is the critical buckling load due to the external compressive load.

Several mesh sizes were used and the results are reported in Table II in terms of non-dimensional critical buckling load. It can be seen that as the power law index increases, the non-dimensional critical buckling load for uniaxial compression loading decreases. It also decreases with increase in porosity for constant size to thickness ratio. For validation and accuracy, the results were compared with the findings of [20]. For a critical buckling load, it has been observed that a mesh size of 13×13 can provide sufficient convergence. Table III gives the critical buckling loads for a square simply supported PFGM plate for biaxial compressive buckling loads. In Table IV, the dimensionless critical buckling load for uniaxial compressive loading is presented for various porosities. A square Al/Al_2O_3 PFGM plate was analyzed for buckling with all sides simply-supported. It has been observed that, with a given size-to-thickness (a/h) ratio, a rise in the porosity results in a gradual decrease in the non-dimensional critical buckling load. It is also observed that an increase in the a/h ratio results in an increase in the critical buckling load. Table V gives the dimensionless critical buckling load for biaxial compressive load. Figure 2 depicts that the Young's modulus decreases as porosity increases. Figure 3 depicts the variation of non-dimensional critical buckling ratio with power index for various porosities for a square plate in the simply supported condition.

TABLE II. NON-DIMENSIONAL UNIAXIAL CRITICAL BUCKLING LOADS FOR VARIOUS POWER LAW EXPONENTS AND POROSITY FOR A SQUARE AL/AL_2O_3 PFGM PLATE

a/h	Remark	ξ = 0.2				ξ = 0.4			
		p=0	p=0.1	p=0.5	p=1	p=0	p=0.1	p=0.5	p=1
10	[20]	17.9991	16.1914	11.4689	8.5746	17.3877	15.5757	10.7802	7.7486
	Present (5×5)	18.1196	16.3440	12.1682	9.8071	17.5063	15.7324	11.5284	9.0943
	Present (7×7)	18.0764	16.3036	12.1293	9.7668	17.4662	15.6949	11.4920	9.0559
	Present (9×9)	18.0657	16.2934	12.1190	9.7557	17.4562	15.6856	11.4823	9.0452
	Present (11×11)	18.0621	16.2900	12.1153	9.7514	17.4529	15.6824	11.4788	9.0410
	Present (13×13)	18.0606	16.2886	12.1136	9.7494	17.4515	15.6810	11.4772	9.0390

TABLE III. NON-DIMENSIONAL BIAXIAL CRITICAL BUCKLING LOADS FOR VARIOUS POWER LAW EXPONENTS AND POROSITY FOR A SQUARE AL/AL_2O_3 PFGM PLATE

a/h	Remark	ξ = 0.2				ξ = 0.4			
		p=0	p=0.1	p=0.5	p=1	p=0	p=0.1	p=0.5	p=1
10	[20]	8.9995	8.0957	5.7344	4.2873	8.6938	7.7894	5.3901	3.8743
	Present (5×5)	9.0598	801720	6.0842	4.9043	8.7531	7.8662	5.7644	4.5483
	Present (7×7)	9.0382	8.1518	6.0648	4.8842	8.7331	7.8474	5.7462	4.5291
	Present (9×9)	9.0329	8.1467	6.0596	4.8787	8.7281	7.8428	5.7414	4.5238
	Present (11×11)	9.0310	8.1450	6.0578	4.8765	8.7264	7.8412	5.7396	4.5217
	Present (13×13)	9.0303	8.1443	6.0569	4.8755	8.7257	7.8405	5.7388	4.5207

TABLE IV. NON-DIMENSIONAL UNIAXIAL CRITICAL BUCKLING LOAD FOR VARIOUS POROSITIES FOR A SQUARE AL/AL_2O_3 PFGM PLATE (p= 0.5)

Boundary condition	a/h	ξ =0	ξ =0.1	ξ =0.3	ξ =0.5
SSSS	5	11.1799	10.8671	10.2275	9.5633
	10	12.7376	12.4269	11.7972	11.1528
	15	13.0766	12.7679	12.1443	11.5094
	20	13.2010	12.8932	12.2719	11.6409
	25	13.2608	12.9533	12.3332	11.7040
	50	13.5202	13.0430	12.4240	11.7968
	100	13.3834	13.0762	12.4573	11.8306

TABLE V. NON-DIMENSIONAL BIAXIAL CRITICAL BUCKLING LOAD FOR VARIOUS POROSITIES FOR A SQUARE AL/AL_2O_3 PFGM PLATE (P= 0.5)

Boundary condition	a/h	ξ =0	ξ =0.1	ξ =0.3	ξ =0.5
SSSS	5	5.5900	5.4336	5.1136	4.7810
	10	6.3689	6.2136	5.8988	5.5766
	15	6.5384	6.3841	6.0723	5.7549
	20	6.6006	6.4467	6.1361	5.8207
	25	6.6305	6.4768	6.1667	5.8522
	50	6.6752	6.5216	6.2121	5.8986
	100	6.6918	6.5382	6.2288	5.9155

IV. CONCLUSIONS

In this paper, buckling analysis of PFGM plate was carried out using FE formulation based on the nine-node isoparametric C_0 continuous shape functions from the proposed displacement fields with hybrid hyperbolic tangent and secant function for accounting the effect of thickness stretching which may arise due to porosity.

The performance of the FE model was assessed as satisfying after comparing the findings with the existing literature. For the parametric study, the model was transformed for different a/h ratio values and porosity distributions. The corresponding critical buckling load for uniaxial and biaxial compressive loading was calculated.

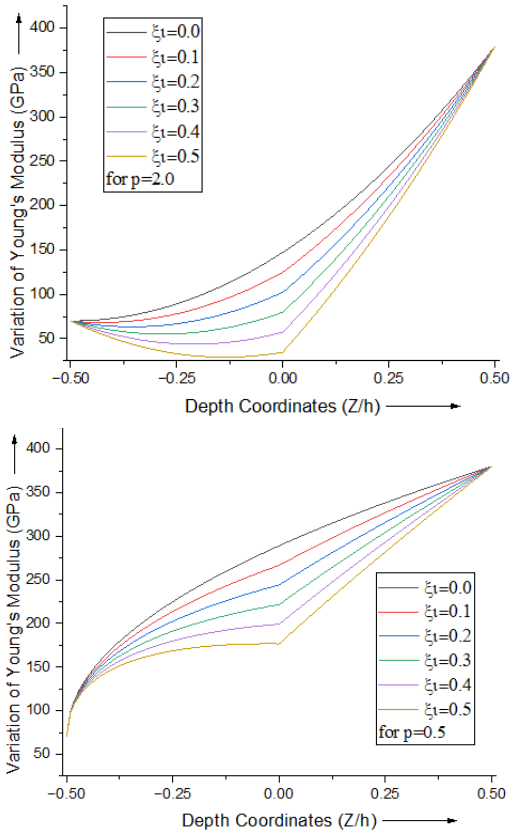

Fig. 2. Variation of Young's modulus with thickness coordinates for various values of porosity and power law indices, (a) p= 2 (b) p = 0.5.

The main drawn conclusions regarding the critical buckling load in buckling analysis are:

- The FE model shows good convergence, producing accurate results, with an optimal mesh size of 13×13.

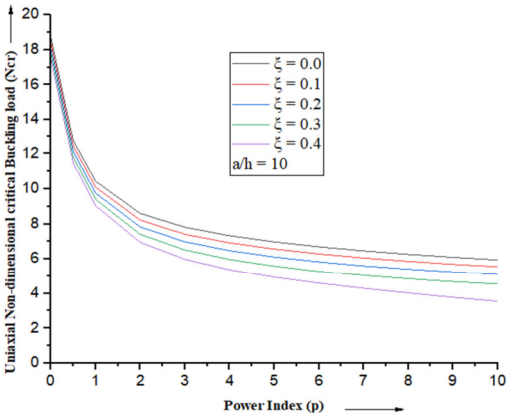

Fig. 3. Variation of the non-dimensional critical buckling ratio with power index for different porosities.

- For the same boundary conditions and plate geometry, the critical buckling load for uniaxial buckling is greater than that for biaxial buckling.
- The percentage error for the FE model is comparable with the existing results.
- There is a strong correlation between the critical buckling load and the ceramic volume fraction. The magnitude of the critical buckling load depends on the ceramic volume fraction, and as it goes down, so does the critical buckling load.
- As the a/h ratio increases, the non-dimensional critical buckling load for constant porosity increases. The net effect of increased porosity is a decrease in stiffness.

REFERENCES

[1] N. T. Hiep, D. S. Dan, N. D. Diem, and D. N. Tien, "NURBS-based Isogeometric Analysis and Refined Plate Theory Application on a Functionally Graded Plate Subjected to Random Loads," *Engineering, Technology & Applied Science Research*, vol. 13, no. 2, pp. 10243–10248, Apr. 2023, https://doi.org/10.48084/etasr.5478.

[2] D. T. Thuy, L. N. Ngoc, D. N. Tien, and H. V. Thanh, "An Analytical Solution for the Dynamics of a Functionally Graded Plate resting on Viscoelastic Foundation," *Engineering, Technology & Applied Science Research*, vol. 13, no. 1, pp. 9926–9931, Feb. 2023, https://doi.org/10.48084/etasr.5420.

[3] D. Chen, J. Yang, and S. Kitipornchai, "Elastic buckling and static bending of shear deformable functionally graded porous beam," *Composite Structures*, vol. 133, pp. 54–61, Dec. 2015, https://doi.org/10.1016/j.compstruct.2015.07.052.

[4] I. Kayabasi, G. Sur, H. Gokkaya, and Y. Sun, "Functionally Graded Material Production and Characterization using the Vertical Separator Molding Technique and the Powder Metallurgy Method," *Engineering, Technology & Applied Science Research*, vol. 12, no. 4, pp. 8785–8790, Aug. 2022, https://doi.org/10.48084/etasr.5025.

[5] M. Avalle, G. Belingardi, and R. Montanini, "Characterization of polymeric structural foams under compressive impact loading by means of energy-absorption diagram," *International Journal of Impact Engineering*, vol. 25, no. 5, pp. 455–472, May 2001, https://doi.org/10.1016/S0734-743X(00)00060-9.

[6] R. Rajendran, K. Prem Sai, B. Chandrasekar, A. Gokhale, and S. Basu, "Preliminary investigation of aluminium foam as an energy absorber for nuclear transportation cask," *Materials & Design*, vol. 29, no. 9, pp. 1732–1739, Oct. 2008, https://doi.org/10.1016/j.matdes.2008.03.028.

[7] Y. F. Zhang, Y. Z. Tang, G. Zhou, J. N. Wei, and F. S. Han, "Dynamic compression properties of porous aluminum," *Materials Letters*, vol. 56, no. 5, pp. 728–731, Nov. 2002, https://doi.org/10.1016/S0167-577X(02)00603-1.

[8] Y. Zhao, M. Taya, Y. Kang, and A. Kawasaki, "Compression behavior of porous NiTi shape memory alloy," *Acta Materialia*, vol. 53, no. 2, pp. 337–343, Jan. 2005, https://doi.org/10.1016/j.actamat.2004.09.029.

[9] P. T. Thang, T. Nguyen-Thoi, D. Lee, J. Kang, and J. Lee, "Elastic buckling and free vibration analyses of porous-cellular plates with uniform and non-uniform porosity distributions," *Aerospace Science and Technology*, vol. 79, pp. 278–287, Aug. 2018, https://doi.org/10.1016/j.ast.2018.06.010.

[10] M. Kamranfard, A. Saidi, and A. Naderi, "Analytical solution for vibration and buckling of annular sectorial porous plates under in-plane uniform compressive loading," *Proceedings of the Institution of Mechanical Engineers, Part C: Journal of Mechanical Engineering Science*, vol. 232, no. 12, pp. 2211–2228, Jun. 2018, https://doi.org/10.1177/0954406217716197.

[11] R. P. Shimpi, "Refined Plate Theory and Its Variants," *AIAA Journal*, vol. 40, no. 1, pp. 137–146, Jan. 2002, https://doi.org/10.2514/2.1622.

[12] S. Merdaci, A. Tounsi, M. S. A. Houari, I. Mechab, H. Hebali, and S. Benyoucef, "Two new refined shear displacement models for functionally graded sandwich plates," *Archive of Applied Mechanics*, vol. 81, no. 11, pp. 1507–1522, Nov. 2011, https://doi.org/10.1007/s00419-010-0497-5.

[13] M. Ameur, A. Tounsi, I. Mechab, and A. A. El Bedia, "A new trigonometric shear deformation theory for bending analysis of functionally graded plates resting on elastic foundations," *KSCE Journal of Civil Engineering*, vol. 15, no. 8, pp. 1405–1414, Nov. 2011, https://doi.org/10.1007/s12205-011-1361-z.

[14] R. Javaheri and M. R. Eslami, "Buckling of Functionally Graded Plates under In-plane Compressive Loading," *ZAMM - Journal of Applied Mathematics and Mechanics / Zeitschrift für Angewandte Mathematik und Mechanik*, vol. 82, no. 4, pp. 277–283, 2002, https://doi.org/10.1002/1521-4001(200204)82:4<277::AID-ZAMM277>3.0.CO;2-Y.

[15] L. S. Ma and T. J. Wang, "Nonlinear bending and post-buckling of a functionally graded circular plate under mechanical and thermal loadings," *International Journal of Solids and Structures*, vol. 40, no. 13, pp. 3311–3330, Jun. 2003, https://doi.org/10.1016/S0020-7683(03)00118-5.

[16] M. R. Barati and A. M. Zenkour, "Investigating post-buckling of geometrically imperfect metal foam nanobeams with symmetric and asymmetric porosity distributions," *Composite Structures*, vol. 182, pp. 91–98, Dec. 2017, https://doi.org/10.1016/j.compstruct.2017.09.008.

[17] A. Mojahedin, M. Jabbari, A. R. Khorshidvand, and M. R. Eslami, "Buckling analysis of functionally graded circular plates made of saturated porous materials based on higher order shear deformation theory," *Thin-Walled Structures*, vol. 99, pp. 83–90, Feb. 2016, https://doi.org/10.1016/j.tws.2015.11.008.

[18] M. Jabbari, M. Hashemitaheri, A. Mojahedin, and M. R. Eslami, "Thermal Buckling Analysis of Functionally Graded Thin Circular Plate Made of Saturated Porous Materials," *Journal of Thermal Stresses*, vol. 37, no. 2, pp. 202–220, Feb. 2014, https://doi.org/10.1080/01495739.2013.839768.

[19] W. Lanhe, "Thermal buckling of a simply supported moderately thick rectangular FGM plate," *Composite Structures*, vol. 64, no. 2, pp. 211–218, May 2004, https://doi.org/10.1016/j.compstruct.2003.08.004.

[20] M. Dhuria, N. Grover, and K. Goyal, "Influence of porosity distribution on static and buckling responses of porous functionally graded plates," *Structures*, vol. 34, pp. 1458–1474, Dec. 2021, https://doi.org/10.1016/j.istruc.2021.08.050.